Int. J. Environ. Sci. Technol. (2016) 13:209–220
DOI 10.1007/s13762-015-0862-6

ORIGINAL PAPER

Photochemical model simulations of air quality for Houston–Galveston–Brazoria area and analysis of ozone–NO_x–hydrocarbon sensitivity

R. R. Kommalapati[1] · **Z. Liang**[2] · **Z. Huque**[3]

Received: 30 July 2014 / Revised: 3 March 2015 / Accepted: 13 July 2015 / Published online: 4 August 2015

Abstract As part of the State Implementation Plan for the Houston–Galveston–Brazoria (HGB) area which has been declared as a non-attainment area, it was required to assess the impacts of pollutant emissions, meteorological conditions, and initial and boundary conditions on air quality. In this study, photochemical model simulations using the Comprehensive Air Quality Model with extensions (CAMx) were conducted for three ozone episodes between May and October of 2006. The CAMx simulations compared fairly well with the hourly average concentrations of ozone measured at the monitoring sites, and the index of agreement (IOA) values for all the three ozone episodes were found greater than 0.65, which proved to be good for CAMx model performance. Both simulated and observed peak ozone concentrations were observed to occur between 12:00 and 15:00 h. The CAMx simulation results showed that there were 68 days where the maximum 8-h mean ozone concentrations exceeded the NAAQS of 75 ppb out of a total of 72 days simulated in the three ozone episodes. For all three episodes, ozone concentrations were highest during the third quarter of the day. The photochemical indicator ratios of hydrogen peroxide (H_2O_2) to nitric acid (HNO_3) ($[H_2O_2]/[HNO_3]$) showed the HGB area to be a nitrogen oxide (NO_x)-sensitive regime for the episodes studied. This indicated that volatile organic compounds (VOCs) are plentiful, and NO_x is the limiting precursor for ozone formation in the HGB area. The plentiful VOCs in this region are possibly produced from industries and refineries in the HGB area.

Keywords Air quality · CAMx · NO_x · Ozone · Photochemical model · Sensitivity analysis · Simulations

Introduction

In the atmosphere, emitted volatile organic compounds (VOCs) and nitrogen oxides (NO_x) generate tropospheric or ground-level ozone in the presence of sunlight with a series of physical and chemical processes. The ozone formation reactions are mainly with hydroxyl radicals (OH) and nitrate radicals (NO_3) and influenced by meteorological conditions (Atkinson 1994; Hwang et al. 2007). The photochemical air quality models, as well as the associated air quality modeling processes, can provide urban- and regional-scale modeling on ozone formation, photochemical behavior, and transport processes. The theoretically physical and chemical processes being addressed in the photochemical models include turbulent transport and diffusion, dry deposition, wet deposition, and kinetics of atmospheric chemistry. The major photochemical model applications are used for assessment of the relative importance of VOC and NO_x emissions control and for establishment of cost-effective approaches for reducing ambient ozone levels at urban and regional scales (Russell and Dennis 2000). The photochemical air quality models have been used for the Lake Michigan ozone study

---

✉ R. R. Kommalapati
rrkommalapati@pvamu.edu

[1] Department of Civil and Environmental Engineering, NSF CREST Center for Energy and Environmental Sustainability, Prairie View A&M University, Prairie View, TX 77446, USA

[2] NSF CREST Center for Energy and Environmental Sustainability, Prairie View A&M University, Prairie View, TX 77446, USA

[3] Department of Mechanical Engineering, NSF CREST Center for Energy and Environmental Sustainability, Prairie View A&M University, Prairie View, TX 77446, USA

(Roberts et al. 1995; Blanchard et al. 1999), the coastal oxidant assessment for southeast Texas study (Blanchard et al. 1995), the San Joaquin Valley air quality study (Blanchard et al. 1997), and the Baltimore-Washington DC area study (Chang et al. 1997). All these studies investigated NO_x and VOC sensitivity to ozone (Blanchard 2000; Hidy 2000; Kleinman 2000).

The predictions for ozone–NO_x–VOC sensitivity are dependent on the photochemical modeling assumptions. Milford et al. (1994) developed an alternative approach for evaluating NO_x–VOC sensitivity by using key photochemical indicator species. This photochemical indicator approach has shown consistently high correlation with simulated NO_x–VOC sensitivity for case studies in Atlanta, New York, Los Angeles, and Lake Michigan region (Sillman et al. 1997). This approach had the drawback of correlation between sensitivity and indicator species being dependent on model assumptions. This drawback may be overcome by using photochemical indicator species ratios, such as hydrogen peroxide and reactive nitrogen species (Sillman 1995). The Sillman (1995) photochemical indicator species ratio method, hereon, referred as Sillman method, helps in determination of the primary driving mechanism for ozone formation by indicating the leading contributor to ozone formation. The sensitivity of ozone formation is based on the atmospheric chemistry mechanisms that are largely dependent on whether NO_x is dominant or reactive organic gases are dominant. The Sillman method noted correlations between NO_x and VOC sensitivity and indicator species ratios to be robust, not affected by changes to model assumptions, and to some extent influenced by solar radiation and aerosol formation. The comparisons between sensitivity model predictions and measured indicator species would provide a powerful tool in the assessment of the relative importance of VOC and NO_x emissions control approaches (Sillman 1999).

Houston–Galveston–Brazoria (HGB) region is located in southeastern Texas and includes Brazoria, Chambers, Fort Bend, Galveston, Harris, Liberty, Montgomery, and Waller Counties. The Houston metropolitan area which has population of 6.22 million is in the center of this region. Compared to other large metropolitan areas in the USA, The Houston area has a large number of industrial, petrochemical refining and chemical manufacturing facilities in addition to the typical urban emission sources of traffic and other human activities. The total VOC emissions from industrial release events in the Houston area were 4.13 million pounds, while the total NO_x emissions from industrial point source release events accounted for 0.31 million pounds in 2003 (Murphy and Allen 2005). Combined with non-event emissions and other urban emission sources, these ozone precursors can have rapid and efficient ozone formation under favorable meteorological conditions of high temperature, high humidity, and low wind speeds which are the typical conditions in Houston area during the summer months. The Texas Commission on Environmental Quality (TCEQ) observed a total of 15 events of highest measured 8-h average ozone concentrations which are labeled as unhealthy level 'Red' in 2008. For example, on October 25, 2008 the highest measured 8-h average was 109 ppb at one of Houston's regional monitoring sites and the highest measured 1-h average was 151 ppb for the hour from 4:00 to 5:00 pm (TCEQ 2011a). In most of these instances, the local air pollutions sources contributed 40–70 % of the measured area 8-h peak ozone concentrations (TCEQ 2011a).

In this study, the research objective was to evaluate the performance of photochemical model simulations on the observed distributions of ozone with CAMx software and to investigate the role of ozone precursors on ozone–NO_x–hydrocarbon sensitivity using Sillman method to identify whether ozone formation in HGB area is a VOC-sensitive or a NO_x-sensitive chemistry-driven regime.

Materials and methods

Model description

The Comprehensive Air quality Model with extensions (CAMx) is employed in this study for assessment of gaseous air pollution in the HGB region. CAMx is an Eulerian photochemical dispersion model and is used to simulate the emission, dispersion, chemical reaction, and removal of pollutants in the troposphere. This model includes transport, turbulent mixing, gas-phase chemistry, aerosol chemistry, dry deposition, wet deposition, and physical and chemical processes. CAMx performs simulations by solving series pollutant continuity equations for each chemical species on a system of nested three-dimensional grids. The series continuity equations used numerical methods for each term of the pollutant continuity equation. The Eulerian continuity equation describes the time dependency of the average species concentration within each grid cell volume as a sum of all of the physical and chemical processes operating on that volume. This equation is expressed mathematically in terrain following height (z) coordinates as shown below (ENVIRON 2011):

$$\frac{\partial C_l}{\partial t} = -\nabla_{\mathrm{H}} \cdot V_{\mathrm{H}} c_l + \left[\frac{\partial (C_l \eta)}{\partial z} - c_l \frac{\partial^2 h}{\partial z \partial t}\right] + \nabla \cdot \rho K \nabla \left({}^{c_l}\!/_{\rho} \right) + \left.\frac{\partial c_l}{\partial t}\right| \text{Emission} + \left.\frac{\partial c_l}{\partial t}\right| \text{Chemistry} + \left.\frac{\partial c_l}{\partial t}\right| \text{Removal}$$

where V_{H} is the horizontal wind vector, c_l is the average species concentration, η is the net vertical transport rate, h is the layer interface height, ρ is atmospheric density, and

K is the turbulent exchange (or diffusion) coefficient. The first term on the right-hand side represents horizontal advection, the second term represents net-resolved vertical transport across an arbitrary space- and time-varying height grid, and the third term represents sub-grid-scale turbulent diffusion. Chemistry is treated by simultaneously solving a set of reaction equations defined from specific chemical mechanisms. Pollutant removal includes both dry surface uptake (deposition) and wet scavenging by precipitation. CAMx uses various chemical mechanisms which contain various reactions from CAMx selected and user-defined reaction equations for its simulation (ENVIRON 2011).

In this study, a geographical region (sub-domain) is identified from a full regional 3D photochemical model. The sub-domain model grids have the same basic structure as a full 3D photochemical grid model. CAMx 4.53 with chemical mechanism CB05 has been used for performing the simulation in this particular study. The full horizontal domain is 2484 km long and 2412 km wide and includes 69 × 67 horizontal coarse grids of 36 × 36 km cells and the nested fine grids of 12 × 12 km cells and 4 × 4 km cells. The vertical configuration of the CAMx modeling domain consists of a varying 28-layer structure above the ground level (AGL) used with the 4 km × 4 km horizontal domain and a varying 17-layered structure used with the 12 km × 12 km and 36 km × 36 km horizontal domains. The 28 vertical layers were up to 15179.1 m above ground level with first layer interface at 33.9 m.

Houston–Galveston–Brazoria monitoring sites

There are over 40 monitoring sites in the HGB area. Twelve of these sites are owned and managed by the TCEQ, and the remaining sites are maintained by the EPA, counties, and other government agencies. The distribution of the monitoring sites in HGB area is shown in Fig. 1. There are 40 ozone monitoring sites in the HGB area (represented by the sky-blue-colored sites in Fig. 1). The measured values at each site can be obtained from the TCEQ Web site in real time. This study used the monitored observations from the 40 sites to evaluate the CAMx-simulated ozone concentrations. (R 2-16)

Validation of models by statistical analysis

The CAMx model performance was evaluated by comparing the model-predicted values with measured values from TCEQ monitoring sites using quantitative and statistical approaches. Three statistical parameters: coefficient of determination, R^2, Pearson correlation coefficient, R, and the "index of agreement" (IOA), d_γ, were employed to measure the CAMx model performance (Willmott 1981, 1982; Willmott et al. 1985).

$$d_\gamma = 1 - \left[\sum_{i=1}^{N} (P_i - O_i)^2\right] \Big/ \left[\sum_{i=1}^{N} (|P_i - \bar{O}|)^2 + (|O_i - \bar{O}|)^2\right]$$

where P_i and O_i are the predicted and measured values, respectively, with a sample size N; and $\bar{O}$ is the average of all measured data. The strength of correlation and dependence between ozone precursors and ozone formation were measured by the Pearson correlation coefficient (R).The analysis of variance (ANOVA) was applied to analyze the model prediction data. The confidence level was set at 95 % for all tests. P values were determined based on paired Student's t test.

Sensitivity test

In the study of Sillman (1995), the ozone–NO_x–VOC sensitivity for ozone formation is attributable to the abundance of the OH radical and the odd-hydrogen cycle. The radical pool of odd hydrogen (HOx) is the sum of OH, HO_2, and RO_2 radicals (Dunker et al. 2002). When NO_x is plentiful, the formation of nitric acid is the main odd-hydrogen radical termination pathway.

$$OH + NO_2 \rightarrow HNO_3$$

Under these conditions, the rate of ozone formation is proportional to the rate of radicals formed which is decreased with increasing NO_x. These conditions are generally described as the VOC-sensitive conditions. Thus, nitric acid (HNO_3) formation is indicative of plentiful NO_x and VOC-sensitive ozone formation.

When NO_x is scarce, the formation of peroxide by radical–radical reaction dominates for odd-hydrogen sink, e.g.,

$$HO_2 + HO_2 \rightarrow H_2O_2 + O_2$$

$$HO_2 + RO_2 \rightarrow ROOH + O_2$$

Under these conditions, ozone formation is limited by the availability of NO to react with HO_2 and RO_2 radicals, which is described as the NO_x-sensitive condition. HO_2 and RO_2 radicals that do not react with NO_x participate in peroxide formation. The rate of ozone formation increases with increasing NO_x and is insensitive to VOC (Sillman 1995).

Sillman (1995) exploited this condition by developing a useful VOC- versus NO_x-sensitive ozone formation based on the ratio of peroxide and nitric acid production. Sillman (1995) proposed that the transition between these/the above-stated two conditions occurs in the range of 0.3–0.6.

$$\left(\frac{P_{H_2O_2} + P_{ROOH}}{P_{HNO_3}}\right) = \text{range of } 0.3 \text{ to } 0.6$$

The production of H_2O_2 and HNO_3 is easily accessible

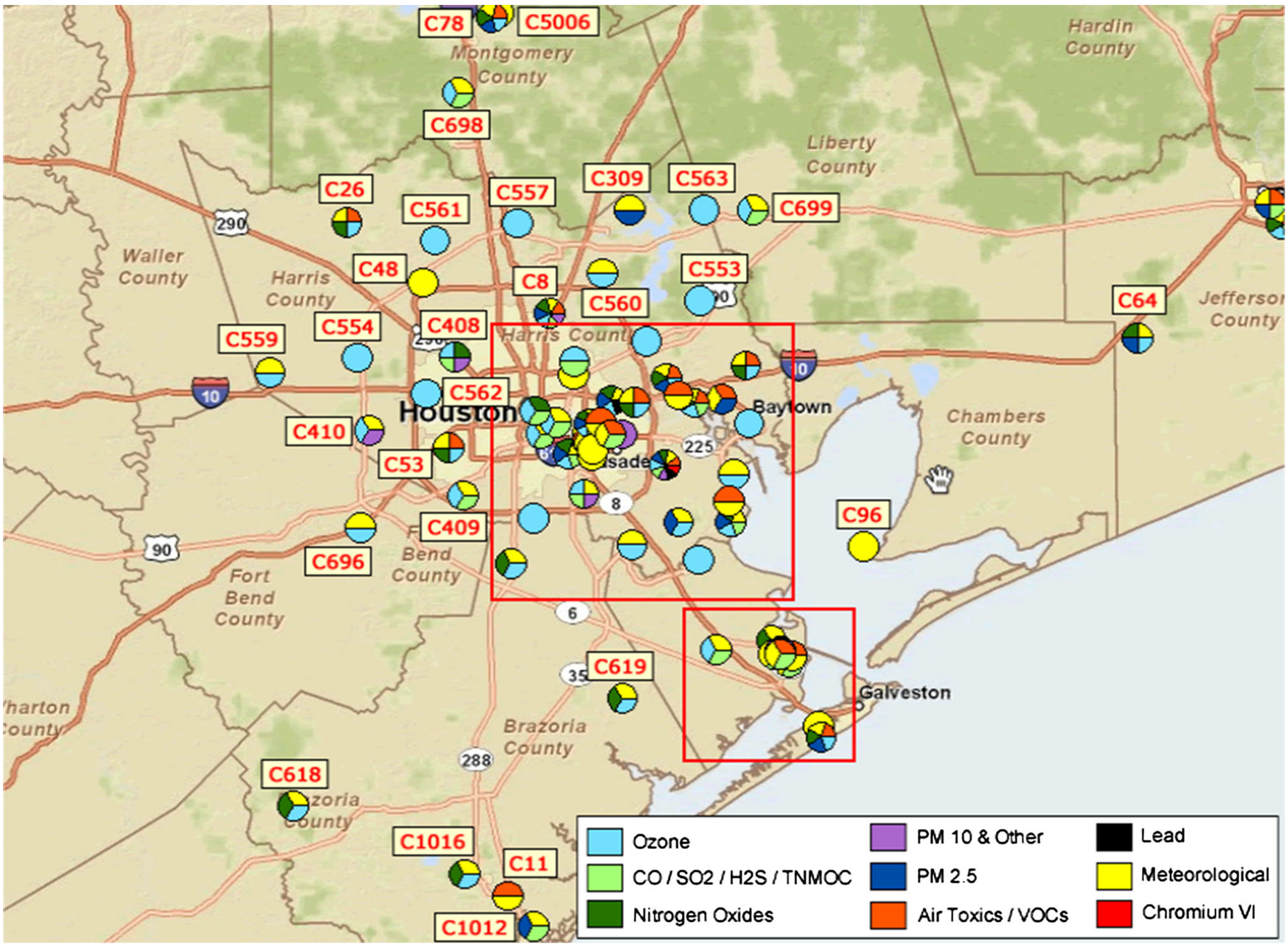

Fig. 1 Air quality monitoring sites in the Houston–Galveston–Brazoria ozone nonattainment area (TCEQ 2011b)

in the CAMx grid, but concentration of ROOH in the grid is under the CB5 chemistry mechanism. The balance between P_{ROOH} and $P_{H_2O_2}$ depends on the relative size of HO_2 and RO_2 radicals. The division into NO_x-sensitive and VOC-sensitive photochemical regimes can be deduced from the H_2O_2/HNO_3 ratio which is dependent on the relative magnitude of odd-hydrogen cycle. For the CAMx simulation, the relative magnitude of the reaction $(P_{H_2O_2}/P_{HNO_3})$ in the model uses the 0.3–0.6 transition point.

The transition from NO_x-sensitive to VOC-sensitive regimes occurs at H_2O_2/HNO_3 ratios in the range of 0.3–0.6. In other words, when this ratio exceeds the 0.3–0.6 range, ozone formation is NO_x sensitive and when this ratio is less than 0.3, ozone formation is VOC limited and NO_x is the compound that dominates the formation of ozone. Since VOC compounds are mostly associated with industries (e.g., refineries and chemical manufacturing industries) and NO_x is majorly associated with combustion sources (e.g., automobiles and large power-generating plants), an indication of the dominant reactions that helps ozone formation can be partially inferred using the Sillman method. The higher values of photochemical indicator species ratios represent a dominant NO_x-sensitive chemistry, while the lower values represent a VOC-dominant chemistry.

Results and discussion

CAMx model results

Figure 2 shows the predicted ground-level ozone concentration at 16:00 h central standard time (CST) on August 22, 2006 using a 4-km grid model resolution in the HGB area, which had the highest ozone concentration of 141 ppb. From Fig. 2, it can be noted that the higher ozone

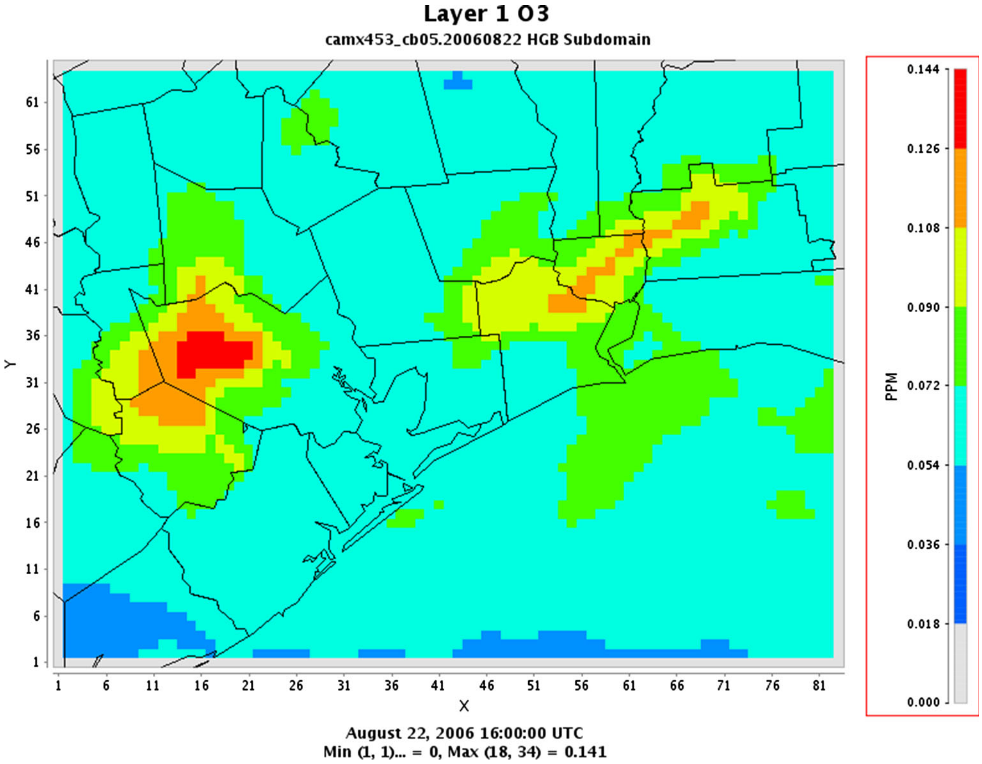

Fig. 2 Ground-level ozone modeled concentrations (ppm) for the 22 August 16:00 CST in the HGB sub-domain (The UTC displayed under the graph is software generated but it is CST)

concentration range of 90–140 ppb mostly covers the Houston metropolitan part of the HGB area at 4 PM. During this time, the solar radiation is strong, temperature is the highest, and photochemical activities are also in the high range. The predicted ozone concentration for the same area ranged from 18 to 36 ppb at 8:00 a.m., which corresponds to the time when the sunlight is weak and ambient temperature just starts increasing. The predicted daily maximum 8-h mean ozone concentration was 103 ppb, and the 8-h concentration contour is overspread on most parts of the Houston metropolitan area. The predicted episode averages of daily maximum 8-h mean ozone concentrations in the HGB area for time periods May 31–June 15, August 13–September 15, and September 16–October 11 of 2006 are 96, 95 and 83 ppb, respectively. Correspondingly, the predicted episode averages of maximum daily 1-h mean ozone concentrations for the three episodes in 2006 are 116, 117, and 95 ppb, respectively. All episode averages for daily maximum 8-h mean ozone concentrations exceeded the standard of 75 ppb set by the National Ambient Air Quality Standards (NAAQS), which is the reason why HGB has been one of the non-attainment areas. The time periods that predicted ozone concentrations exceeding the 75 ppb limit for most of the days in the episodes were between 12 noon and 8 p.m. Only 4 days of predicted daily maximum 8-h mean ozone concentrations were below the 75 ppb limit, and the 4 days occurred in the September–October episode on September 19, 20, 25, and October 10. The meteorological conditions for these 4 days showed characteristics of relatively lower humidity and temperature.

The consecutive hourly CAMx model-predicted versus observed ozone concentrations from the 40 TCEQ monitoring sites in the HGB sub-domain during the May 31–June 15, 2006 episode are shown in Fig. 3. The CAMx model prediction replicated the diurnal rise and fall of ozone concentrations quite well for all days in the episode. Figure 3 also shows that the ozone concentrations are usually above the 75-ppb standard (as seen by the peaks) every day during the hours of 11 a.m. and 5 p.m. Both simulated and observed peak ozone concentrations occur between 12 noon and 3 p.m. when solar radiation and ambient temperatures are the highest during the daytime. This demonstrated that the observed ozone pattern is well predicted by the CAMx model simulations, and the peak ozone concentrations are properly predicted. However, for the time period from 11 p.m. to 7 a.m., CAMx model-predicted ozone concentrations were higher than the observed TCEQ ozone concentrations. This might be due to the background ozone concentration setting used in

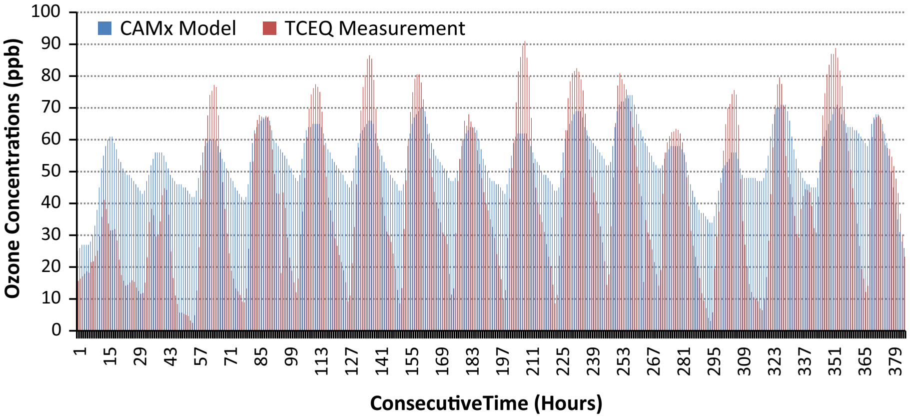

Fig. 3 Consecutive hourly predicted and observed ozone concentrations at HGB area during the May 31–June 15, 2006 episode

Table 1 Statistical analysis of CAMx model performance

Episode	R	R^2	d_γ	N
May–June (Spring)	0.78	0.60	0.68	384
August (Summer)	0.83	0.68	0.71	192
October (Autumn)	0.85	0.72	0.66	216

CAMx model simulations. The comparison of consecutive hourly CAMx model-predicted versus observed ozone concentrations for episodes of August and October was also similar to the results presented in Fig. 3. The CAMx model performance on hourly ozone concentration forecasts was measured by the correlation coefficient (R), coefficient of determination (R^2), and the index of agreement (d_γ) as presented in Table 1. The performance results shown in Table 1 included the CAMx model simulations for 16 consecutive days, 8 consecutive days, and 10 consecutive days during May, August, and October ozone episodes at 40 monitoring sites in the HGB area. The correlation coefficients between modeled and observed hourly averaged values are 0.78, 0.83, and 0.85 for May, August, and October episodes, respectively. The coefficient of determination for May, August, and October episodes between modeled and observed hourly averaged values are 0.6, 0.68, and 0.72, respectively. The index of agreements (IOA) which measures the degree of prediction deviations from observed values are 0.68, 0.71, and 0.66 for May, August, and October episodes, respectively. The IOA values for all the episodes forecasted were significantly greater than 0.65 indicating good agreement between CAMx model predictions and observed TCEQ values.

Ozone–NO_x–VOC sensitivity analysis

Figure 4 shows the modeled ozone concentration and H_2O_2 concentration for representative (a) morning, (b) afternoon, and (c) evening time periods. Ozone concentration showed a good correlation with H_2O_2 concentration in the morning (refer Fig. 4). The slope from an O_3–H_2O_2 linear regression is 5.16, and this represents the number of ozone molecules formed per H_2O_2 produced. The Pearson correlation coefficient calculated from Fig. 4 in the morning is 0.86. The values of O_3–H_2O_2 slope for other days morning O_3–H_2O_2 linear regression ranged from 3.67 to 13.58 with average R^2 value of 0.696. Figure 5 shows the scatter plot of simulated ozone concentration and HNO_3 concentration during representative (a) morning, (b) afternoon, and (c) evening time periods. The ozone concentration generally increased from the morning to peak concentration between 2 p.m. and 4 p.m. in the afternoon with increasing HNO_3 concentrations. The maximum ozone concentration of 91.4 ppb and HNO_3 scatter plot confirmed that the CAMx-simulated maximum ozone concentration of 91 ppb for August 30, 2006. From Fig. 5, one can note the ozone concentration to have a strong correlation with HNO_3 concentration in the afternoon. The slope from an O_3–HNO_3 linear regression is 19.42 and represented as ozone yield estimation and the Pearson correlation coefficient calculated from Fig. 5b is 0.95 with sample size (N) of 5102. The values of O_3–HNO_3 slope for other daily's afternoon O_3–HNO_3 linear regression ranged from 5.67 to 19.42 with average R^2 value of 0.701.

The variation of linear regression slopes and the R^2 values for ozone versus H_2O_2 and ozone versus HNO_3 over a selected day are shown in Fig. 6a, b, respectively. Identical variations are noted for all other days in the three ozone episodes. The morning O_3–H_2O_2 linear regression R^2 values are significantly higher than those in the afternoon and evening times (refer Fig. 6a). The positive correlation for the morning time ozone formation reflected that the fresh ozone formation is corresponding with the urban VOC emission sources due to the abundant human activities in the morning such as morning commute. The results of O_3–HNO_3 linear regression slope and R^2 showed a very

Fig. 4 CAMx-simulated ozone concentration versus H_2O_2 concentration for selected date of August 19, 2006 **a** 09:00, **b** 15:00, and **c** 22:00 CST

good correlation in the afternoon compared to morning and evening hours (refer Fig. 6b). As pointed out by Sillman (1995), H_2O_2 is the photochemical indicator for hydrocarbons, and HNO_3 is a photochemical indicator for NO_x. The strong correlation between ozone and H_2O_2 in the morning hours and a strong correlation between ozone and HNO_3 in the afternoon were suggested by Sillman (1995) as well. The ozone formation dependency is moving from O_3–H_2O_2 dependency in the morning time toward the O_3-HNO_3 dependency in the afternoon time with higher range of ozone yield estimation. This comparison confirmed the well-accepted fact that in urban areas the freshly emitted air pollutants in the mornings usually are characterized as VOC control regime because of low levels of solar radiation that move to a NO_x-limited regime later in the day with air pollutants transport and higher photochemical activities (Sillman 1999).

Correlations between the photochemical indicator species of H_2O_2 and HNO_3 concentrations also exhibited a strong correlation in the afternoon compared to morning or evening hours. Similar trends were observed with the slopes of indicator species in the afternoon, being distinctly negative than those slopes in the morning. The simulated strong correlations between indicator species strengthened the connection between ozone–NO_x–VOC sensitivity and indicator species. The negative correlations and slopes

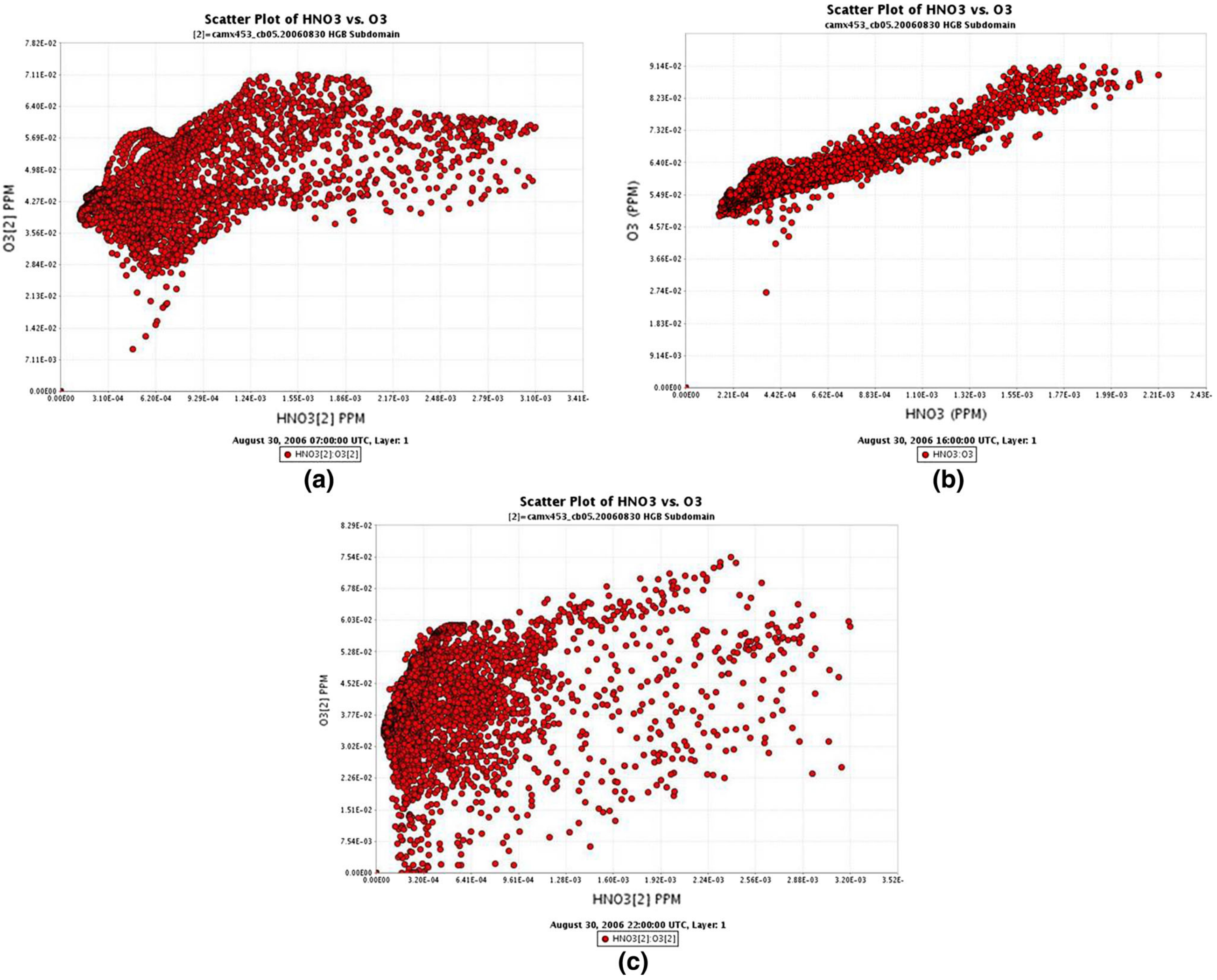

Fig. 5 CAMx-simulated ozone concentration versus HNO_3 concentration for selected date of August 30, 2006 **a** 07:00, **b** 16:00, and **c** 22:00 CST

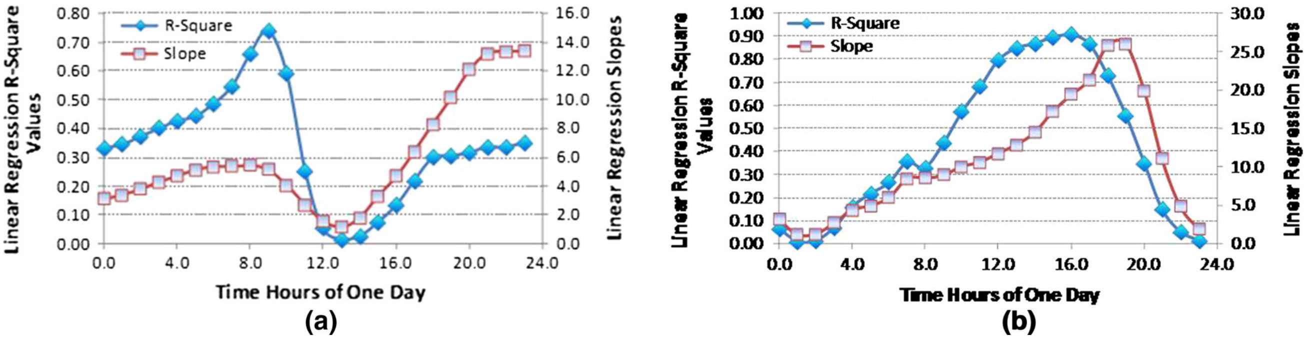

Fig. 6 Coefficients of determination and linear regression slopes for **a** O_3–H_2O_2 linear regression for August 19, 2006 and **b** O_3–HNO_3 linear regression for August 30, 2006

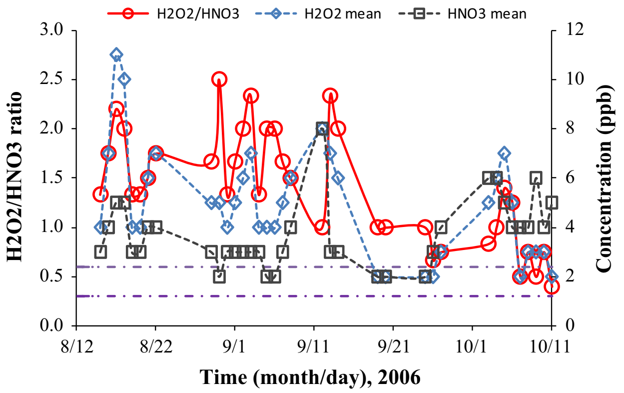

Fig. 7 Daily H_2O_2/HNO_3 ratio in the CAMx simulation for HGB sub-domain. The area between the *dashed horizontal lines* represents the transition regime

between H_2O_2 and HNO_3 species demonstrated that increased formation of HNO_3 as a NO_x sink with decreasing H_2O_2 production as an indicator of NO_x-sensitive chemistry. During this phase, NO_x actively participated in the ozone production while acting as catalyst for the VOC degradation. These distinct slopes between indicator species confirmed the movement toward NO_x-sensitive chemistry. These distinct slopes might represent the difference in combined usual urban emission sources and industrial emissions in the photochemical evolution of chemical sensitivity.

Figure 7 shows the daily ratio of H_2O_2/HNO_3 from the CAMx simulation for HGB sub-domain for episodes of August–September, and September–October and the daily—average indicator species of H_2O_2 and HNO_3 concentration for the same period. As can be seen from Fig. 7, the H_2O_2 mean concentrations are consistently higher than HNO_3 mean concentrations for the episode of August–September. The variations of HNO_3 mean concentrations are relatively constant compared to the bigger variation for H_2O_2 mean concentrations. The H_2O_2/HNO_3 ratio is consistently higher than 1.0 and mostly determined by H_2O_2 mean concentrations. The average H_2O_2 mean concentration is 5.86 ppb, and the average HNO_3 mean concentration is 3.45 ppb. The corresponding average H_2O_2/HNO_3 ratio is 1.75. The bigger variation of H_2O_2 mean concentrations indicated that there are a couple of significant industrial VOC emission events that occurred in the HGB region. The model simulation results of indicator species and ratio for the episode of May–June are similar with average H_2O_2 mean concentration, average HNO_3 mean concentration, and corresponding average H_2O_2/HNO_3 ratio of 6.06 ppb, 3.31 ppb, and 1.89, respectively. The results for episode of October are slightly different in that the average H_2O_2 concentration, average HNO_3 concentration and average H_2O_2/HNO_3 ratio are 3.36 ppb, 4.07 ppb, and 0.84. For all episodes, H_2O_2/HNO_3 ratios are consistently higher than the threshold values of $H_2O_2/HNO_3 = 0.3–0.6$ (Sillman 1995, Sillman et al. 1997). The significant values above the threshold ratio indicate a NO_x-sensitive regime in spring, summer, and autumn seasons in the HGB region. Based on the Sillman method guidance that higher values of photochemical indicator species ratios represent a dominant NO_x-sensitive chemistry and lower values represent a VOC-dominant chemistry, ozone formation in the HGB area may be designated to be NO_x sensitive due to higher H_2O_2/HNO_3 ratios.

Table 2 Episode average O_3 concentrations, air temperature, relative humidity, and wind speed

Episode	Max_8h_Mean O_3 (ppb)	Maximum O_3 (ppb)	Temperature (°C)	Relative humidity (%)	Wind speed (m/s)
June	96.50 ± 9.19	115.9 ± 13.6	26.91 ± 1.54	66.33 ± 8.58	2.62 ± 0.81
August	95.45 ± 13.6	117.5 ± 19.9	27.60 ± 2.03	66.35 ± 6.72	1.88 ± 0.60
October	82.79 ± 10.4	95.29 ± 12.4	23.51 ± 1.98	66.38 ± 8.76	2.10 ± 0.76

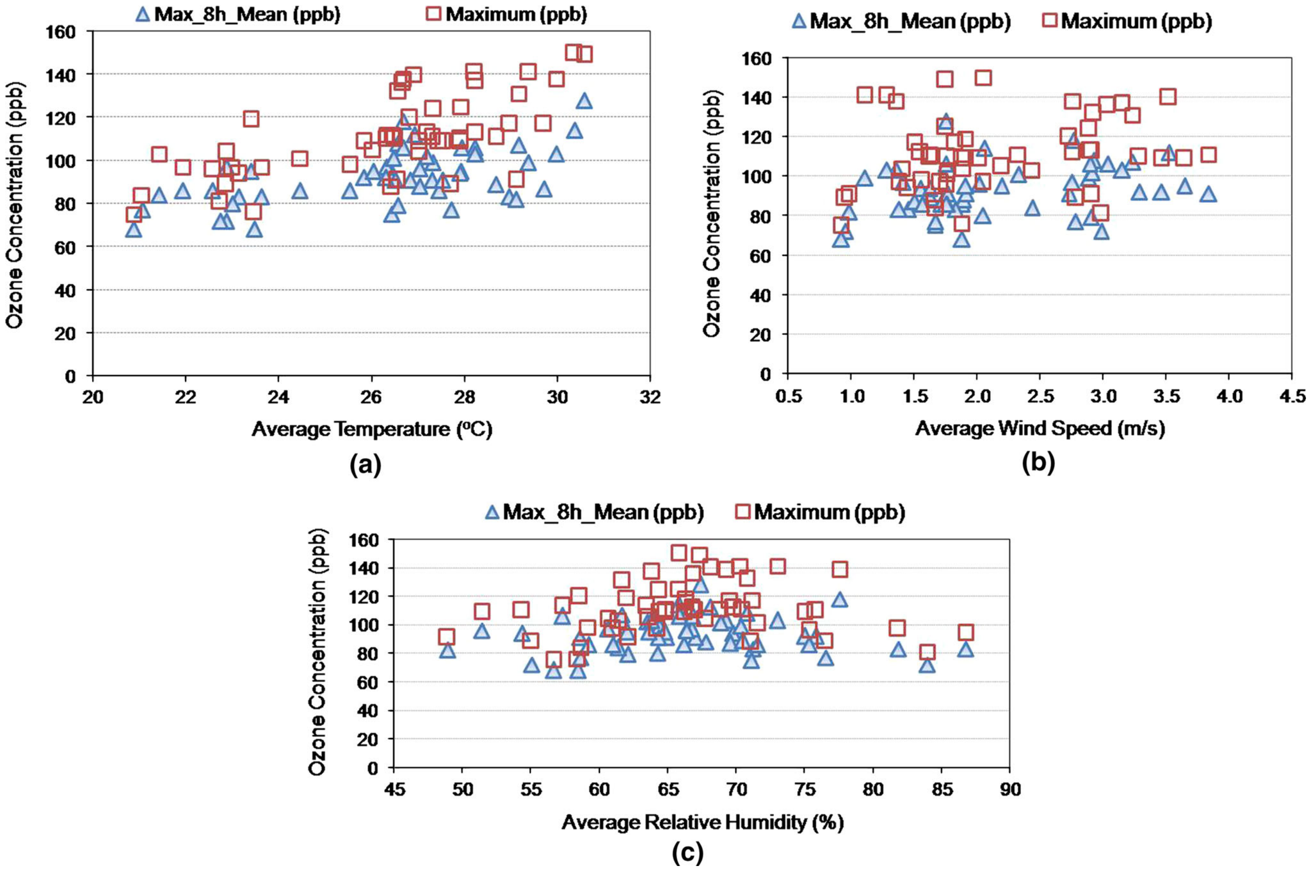

Fig. 8 Daily modeled maximum 8-h mean ozone concentration and maximum ozone concentration as a function of **a** temperature **b** wind speed and **c** relative humidity for the three episodes

Meteorological effects on ozone formation

Meteorological conditions such as temperature, wind speed, solar radiation, and relative humidity have significant influence on ozone formation, transfer, and dispersion. Temperature is the key variable which has the highest impact on the stability of atmosphere and growth of the boundary layer. The photochemical reaction rates along with mobile and biogenic emission sources are also temperature dependent. Wind speed influences air pollutant mixing and transport across the modeling domain. Relative humidity and solar radiation also influence the photolysis rates and the spatial and temporal distribution of ozone formation. Table 2 summarizes the average episode variations of ozone concentrations with air temperature, wind speed, and relative humidity for all three ozone episodes studied. The variations of daily maximum 8-h mean ozone concentrations and daily maximum 1-h ozone concentrations with individual meteorological parameters of temperature, wind speed, and relative humidity are shown in Fig. 8. The highest ozone concentration was about 117.5 ± 19.9 ppb in August with high air temperature of 27.6 °C. Regression analysis of the daily averaged and maximum ozone concentration was performed to quantitatively assess the influence of meteorological factors on ozone formation (refer Fig. 8). A positive correlation coefficient of 0.591 was obtained for ozone and temperature. The significant correlation between ozone and temperature could be explained by the fact that high temperature enhances the solar energy that increases ozone production. The correlation between wind speed and ozone is positive (refer Fig. 8) and weak with a low regression value of 0.311. High wind speeds result in rapid mixing of primary pollutants which leads to high ozone concentrations. Also, higher wind speeds facilitate less chemical loss of ozone. The correlation between relative humidity and ozone was not significant with a correlation value of 0.05 (refer Fig. 8). The relative humidity for all three ozone episodes was nearly constant at 66.3 % (from Table 2). Hence, the effect of relative humidity on ozone formation can be termed insignificant.

Conclusion

The performance of photochemical model simulations for ozone distribution in the HGB area was evaluated with CAMx for three episodes in late spring, summer, and early fall. Averages of daily maximum 8-h mean ozone modeled concentrations exceeded the NAAQS standard of 75 ppb for all episodes studied in the HGB area that was labeled as a non-attainment area. CAMx model simulations predicated the observed ozone patterns well as indicated by the index of agreement. Both simulated and observed peak ozone concentrations occurred between 12 noon and 3 p.m. when solar radiation and ambient temperature were found to be the highest.

The ozone formation dependency moved from O_3–H_2O_2 dependency in the morning to O_3–HNO_3 dependency in the afternoon. This comparison confirmed that ozone formation is characterized as VOC control regime with less solar radiation in the morning time and NO_x-limited regime with higher air pollutants transport and photochemical activities in the afternoon. For all three ozone episodes, the photochemical indicator species ratio of H_2O_2/HNO_3 from the CAMx simulation was consistently higher than the threshold values (0.3–0.6) for H_2O_2/HNO_3 indicating a NO_x-sensitive regime in the HGB region. The meteorological variables of temperature and wind speed showed positive correlation with ozone concentrations, while relative humidity had no correlation.

Acknowledgments This work is supported by the National Science Foundation (NSF) through the Center for Energy and Environmental Sustainability (CEES), a NSF CREST Center award #1036593.

References

Atkinson R (1994) Kinetics and mechanisms of the gas-phase reactions of the hydroxyl radical with organic compounds. J Phys Chem Ref Data Monogr 2:1–216

Blanchard CL (2000) Ozone process insights from field experiments—part III: extent of reaction and ozone formation. Atmos Environ 34:2035–2043

Blanchard CL, Roberts PT, Chinkin LR, Roth PM (1995) Application of smog production (SP) algorithms to the TNRCC COAST data. Pages paper 95-TP15P.04. In: 86th annual meeting of the Air and Waste Management Association, San Antonio, TX

Blanchard CL, Roth PM, Tanenbaum SJ (1997) Development of a method for determining if the control of VOC or NO_x is likely to be more effective for reducing ozone concentrations. In: American Petroleum Institute, Washington, DC

Blanchard CL, Lurmann FW, Roth PM, Jeffries HE, Korc M (1999) The use of ambient data to corroborate analyses of ozone control strategies. Atmos Environ 33:369–381

Chang TY, Chock DP, Nance BI, Winkler SL (1997) A photochemical extent parameter to aid ozone air quality management. Atmos Environ 31:2787–2794

Dunker AM, Yarwood G, Ortmann JP, Wilson GM (2002) Comparison of source apportionment and source sensitivity of ozone in a three-dimensional air quality model. Environ Sci Technol 36:2953–2964

ENVIRON (2011) CAMx user's guide comprehensive air quality model with extensions version 5.40. Novato, CA

Hidy GM (2000) Ozone process insights from field experiments—part I: overview. Atmos Environ 34:2001–2022

Hwang MK, Kim YK, Oh IB, Hwa WL, Kim CH (2007) Identification and interpretation of representative ozone distributions in association with the sea breeze from different synoptic winds over the Coastal Urban Area in Korea. J Air Waste Manag Assoc 57:1480–1488

Kleinman LI (2000) Ozone process insights from field experiments—part II: observation-based analysis for ozone production. Atmos Environ 34:2023–2033

Milford JB, Dongfen G, Sillman S, Blossey P, Russell AG (1994) Total reactive nitrogen (NO_y) as an indicator of the sensitivity of ozone to reductions in hydrocarbon and NO_x emissions. J Geophys Res 99:3533–3542

Murphy CF, Allen DT (2005) Hydrocarbon emissions from industrial release events in the Houston-Galveston area and their impact on ozone formation. Atmos Environ 39:3785–3798

Roberts PT, Roth PM, Blanchard CL, Korc ME, Lurmann FW (1995) Characteristics of VOC-limited and NO_x-limited areas within the lake michigan air quality region. In: Lake Michigan air directors consortium, Des Plaines, IL

Russell A, Dennis R (2000) NARSTO critical review of photochemical models and modeling. Atmos Environ 34:2283–2324

Sillman S (1995) The use of NO_y, H_2O_2, and HNO_3 as indicators for ozone–NO_x–hydrocarbon sensitivity in urban locations. J Geophys Res 100:14175–114188

Sillman S (1999) The relation between ozone, NO(x) and hydrocarbons in urban and polluted rural environments. Atmos Environ 33:1821–1845

Sillman S, He D, Cardelino C, Imhoff RE (1997) The use of photochemical indicators to evaluate ozone–NO_x–hydrocarbon sensitivity: case studies from Atlanta, New York, and Los Angeles. J Air Waste Manag Assoc 47:1030–1040

TCEQ (2011a) 2008 Air pollution events. http://www.tceq.texas.gov/airquality/monops/sigevents08.html.in. T. C. E. Q. editor

TCEQ (2011b) Air quality monitoring sites in the Houston–Galveston–Brazoria ozone nonattainment area. http://www.tceq.texas.gov/airquality/airmod/data/hgb8h2/hgb8h2_site.html#sites

Willmott CJ (1981) On the validation of models. Phys Geogr 2:184–194

Willmott CJ (1982) Some comments on the evaluation of model performance. Bull Am Meteorol Soc 63:1309–1313

Willmott CJ, Ackleson SG, Davis RE, Feddema JJ, Legates DR, Klink KM, ‘Donnell JO, Rowe CM (1985) Statistics for the evaluation and comparison of models. J Geophys Res 90:8995–9005